Webology (ISSN: 1735-188X)
Volume 18, Number 4, 2021

Classification Of Hyperspectral Images Using Densenet-264 With Tensorflow

G. Narendra[1], Dr. D. Siva kumar[2]

[1]Research Scholar, Department of Electronics & Instrumentation Engineering, Annamalai University, Annamalainagar, Tamil Nadu, India

[2]Professor, Department of Electronics & Instrumentation Engineering, Annamalai University, Annamalainagar, Tamil Nadu, India

Abstract

The DenseNet-264 uses an additive principle to merge the previous layer with the next layer and further it concatenates the previous layer output with next layer. This DenseNet-264 model improves the declined accuracy produced due to vanishing gradients in case of high-level neural network. Hence, the information is preserved in longer paths between the source layer and destination layer without getting vanished in between the layers. In this paper, we study the DenseNet-264 top-5 metric to classify the Hyper-Spectral Image (HSI) features from the input HSI. The simulation is conducted on several HSI images to test the efficacy of the model against various datasets, and the results of simulation shows that the proposed method achieves 99% accuracy than the other existing classifier.

Keywords: Classification, Hyperspectral Image, DenseNet-264, Tensorflow

1. Introduction

In existing image spectrometers, the combination of spectroscopy and image technologies enables the acquisition of different wavelength channels in different locations in an imaging plane of spatially-spectral properties that capture the visible and solar-reflected infrared and short-wellness infrastructure. This image plane is commonly produced by airborne spectrometers [1], particularly in the remote sensor sector, which provide massive volumes of data per hour, frequently close to the information gyrate, while simultaneously improving spatial resolution. In other words, the image plane produces a large amount of data.

For example, the Airborne Visible Infrared Imaging Spectrometer (AVIRIS) [2] provides continuous spectrum coverage at 10 nm intervals across the spectrum, with a range of information spanning from 0.4 to 2.45 m in 224 spectral bands. Another well-known aerial spectrometer is the Reflective Optics System Imaging Spectrometer (ROSIS-3) [3], which covers a range of 0.43–0.86 m and has over 100 spectral bands at 4 nm intervals.

The study of patterns has been a significant focus of HSI categorization for decades, and as a result, a large number of research findings have been generated. In previous works, the methodologies of spectral feature, spatial feature, and spectral-spatial feature extraction have all been presented [12]. One of the earliest and most fundamental constituent parts of a picture is its spectrum feature, which is also known as either the spectral vector or the spectral curve. The spatial feature [13] also refers to the connection between the core pixel and the surrounding area, which has the potential to dramatically improve the model resistance to failure.

At the beginning of the research on HSI classification, pure spectral feature-based approaches were used to classify HSI images. These approaches simply apply classifiers to pixel vectors to produce classification results without any feature extraction and were used in the beginning of the research on HSI classification. In contrast, because of the non-linear relationship between spectra and ground objects, classifying models using raw spectra proves to be more difficult than previously thought. As a result, the emphasis on dimension reduction and feature extraction has increased in more recent methodologies as a result of this. In order to reduce the number of dimensions, some of the most widely used. Despite this, the models' overall performance continues to be subpar.

From hyperspectral images, we can tell that distinct surface items can sometimes have the same spectral characteristic and that the same surface objects can occasionally have different spectral characteristics when compared to one another. A variety of factors influence the spectra of ground objects, including lighting, ambient, atmospheric, and temporal variables.As a result, there is an increased likelihood of misclassification. Therefore, these algorithms rely entirely on spectral information, which results in suboptimal classification results. When it comes to improving classification accuracy and approach resilience, the spatial characteristics of ground objects provide extensive information on shape, context, and layout regarding ground objects and neighbouring pixels are likely members of the same class, which can be used to improve classification accuracy and approach resilience.

The spectrum collection of nband-images in narrow and continuous spectral bands is the information acquired by spectrometers in imaging [4]-[5]. In hyperspectral images, the nbands parameter is typically in the hundreds or thousands, embracing a vast spectral frequency range [6]. As a result, each pixel has a unique spectral signature that provides a highly detailed and distinct reflection of each captured land cover. This resulted in the development of hyper-spectral image (HSI) as a tool for analysing the earth surface for a variety of purposes, offering greater discrimination among the many materials contained in the image. Classification [7], spectral

unmixing [8], target recognition and anomaly detection [9], and HSI analysis are some of the methods used. In recent years, HSI categorization has emerged as a key topic in the area of remote sensing [10].

In this paper, we study the DenseNet-264 top-5 metric to classify the Hyper-Spectral Image (HSI) features from the input HSI. The DenseNet-264 uses an additive principle to merge the previous layer with the next layer and further it concatenates the previous layer output with next layer.

2. Related Works

In the literature, some unsupervised pixel classification devices show good classification precision performance. Uncontrolled approaches, on the other hand, do not require labelled data, which is classed based on the inherent similarities in the data structure, which is generally quantified as the distance between samples and proportionally separated into groups, with each group assigned a label. The most representative unsupervised approaches are KNN [11] and the iterative self-organizing algorithm of data analysis.

Support Vectors Machine (SVM) [13] and Logistic Regression [12], which can accurately perform in the presence of a small set of training settings where the former can easily model a post office, are popularly monitored methods: decision trees (DTs) and random forests (RFs), which have previously been successful in providing good and accurate land cover maps. These approach issues are exacerbated by the high spectral dimension of the HSI data and the limited availability of workout samples. In reality, the supervision category gradually increases with the rise in spectral bands but drops considerably when the nbands exceed a certain limit, necessitating the use of dimensional reduction procedures to reduce the nbands.

Traditional categorization systems have some limitations when compared to ANNs. ANNs have more flexible structures that can handle much larger data sets without the need for prior knowledge of statistical data distribution. They have a strong ability to generalise. The HSI data classification garnered a lot of interest in this area since it was able to create more abstract data visualisations hierarchically from the original data [14]. In other words, DNNs learn basic characteristics in the early layers and develop more intricate ones in the last (high-level) layers by combining the simpler ones [15].

Convolutional neural networks (CNNs) in particular have become a deeply representational model because of their feature detection power, which greatly enhances item categorization and detection [16]. As a result, the CNN obtains good generality in HSI classification [17].

Since its inception a decade ago, deep learning has experienced rapid growth and garnered widespread attention from researchers and industry leaders alike. As opposed to the standard machine learning paradigm, which involves developing feature patterns from start, deep learning technology makes use of data to learn feature patterns on its own. It has just recently been made

available in the HSI classification field as well. Researchers have presented a number of novel deep learning-based HIS classification algorithms that are both effective and efficient.

It is required to provide a large number of training examples with deep learning in order to correctly train the model and modify the model parameters. Because it demands specialised knowledge, and there is not enough training available, labelling by hand is time-consuming and expensive in the real world.

3. Proposed Model

The DenseNet-264 uses an additive principle to merge the previous layer with the next layer and further it concatenates the previous layer output with next layer. DenseNet-264 improves the accuracy that helps in classifying the instances from the HSI images.

Feature Space

After translating the data into feature space, the dot product can be used to establish a similarity measure between two sets of data. As long as the feature space is selected appropriately, pattern recognition becomes straightforward.

$$\langle x_1 \cdot x_2 \rangle \leftarrow K(x_1, x_2) = \langle \Phi(x_1) \cdot \Phi(x_2) \rangle$$

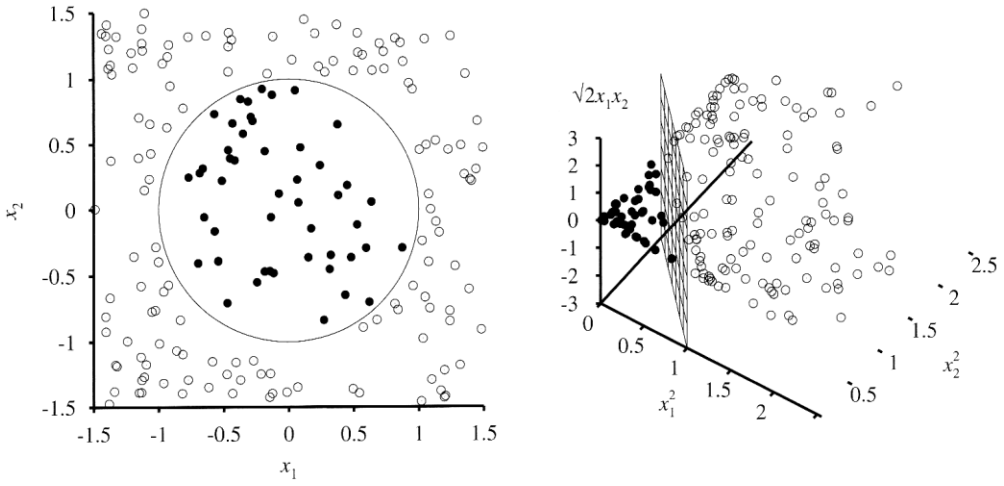

Figure 1: Feature Space Representation

DenseNet-264

Consider the following scenario: x_0 is a single image that has been processed by a neural network. The network consists of L layers, each of which conducts a non-linear transformation H_l, where l denotes the layer as in Figure 1.

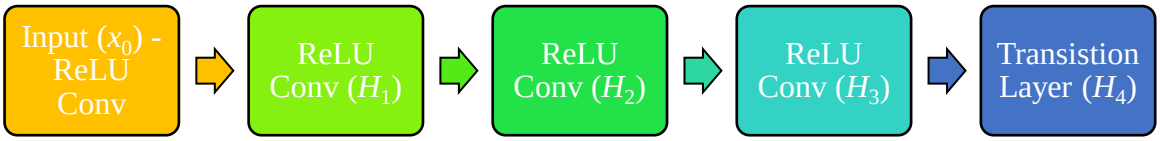

Figure 2: DenseNet-264 architecture

ResNets.

The output of the l^{th} layer is sent into the (l+1) th layer in traditional convolutional feed-forward networks [16], resulting in the layer transition $x_l = H_l(x_l\text{-}1)$. ResNets include a skip-connection that avoids the identity function non-linear transformations:

$x\ell = H\ell(x\ell-1) + x\ell-1$. (1)

One advantage of ResNets is that the gradient can flow straight from later layers to earlier levels through the identity function. However, the summing of the identity function and the output of H_l may obstruct information flow in the network.

Dense connectivity.

We suggest a novel connectivity pattern to increase information flow across levels: we add direct connections from any layer to all following layers. The conceptual layout of the resulting DenseNet is shown in Figure 1. Consequently, the ℓ th layer receives the feature-maps of all preceding layers, x0, . . . , $x\ell-1$, as input:

$x\ell = H\ell([x0, x1, . . . , x\ell-1])$, (2)

where [x0, x1, . . . , $x\ell-1$] refers to the concatenation of the feature-maps produced in layers 0, . . . , $\ell-1$.

This network architecture is known as a Dense Convolutional Network because of its dense connectedness (DenseNet). We concatenate the numerous inputs of $H_l()$ in Eq.(2) into a single tensor for ease of implementation.

Composite function.

We define $H_l()$ as a composite function of three sequential operations: batch normalisation (BN), rectified linear unit (ReLU), and 3x3 convolution (Conv).

Pooling layers.

When the size of feature-maps changes, the concatenation method in Eq. (2) becomes impractical. However, down-sampling layers that alter the size of feature-maps are a crucial part of convolutional networks. To aid downsampling, our architecture divides the network into multiple tightly connected, dense units. Transition layers are layers that exist between blocks and

conduct convolution and pooling. In our experiments, we used a batch normalisation layer, a 1 x 1 convolutional layer, and a 2 x 2 average pooling layer as transition layers.

Growth rate.

If each function H_l creates kfeaturemaps, the l^{th} layer will have $k_0 + k \times (l-1)$ input featuremaps, where k_0 is the channel count. DenseNet differs from existing network topologies in that it allows for extremely tiny layers, such as k = 12. The hyperparameter k refers to the rate of network growth. According to one interpretation, each layer in its block has access to all of the feature-maps that came before it. The feature-maps represent the general state. This state is made up of k feature-maps contributed by each layer. The rate of expansion affects how much new information each layer contributes to the overall state. The global state may be accessible from anywhere in the network once it is written, and there is no need to transfer it from layer to layer as in typical network topologies.

An early class of algorithms was developed in order to achieve a precise match between the data and the model, in order to provide hypotheses that correctly classified the training data. Generalization refers to a hypothesis's capacity to accurately classify data that is not included in the training data set. Because it inhibits over-generalization, DenseNet outperforms neural networks that are prone to over-generalization in terms of performance. More information may be found in the graphic (Figure 3) on how to find the best trade-off between complexity and the number of epochs.

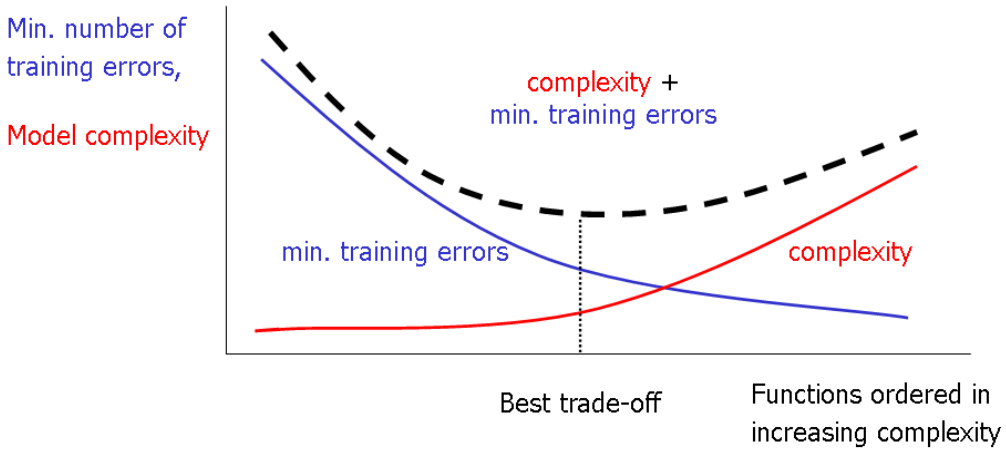

Figure 3: Complexity with growth rate

Bottleneck layers.

Despite the fact that each layer produces k just a few output feature-maps, it typically has a huge number of inputs. 1 x 1 convolution can be used as a bottleneck layer to reduce the number of input feature-maps and thus improve computing performance.

Compression.

To increase model compactness even further, we can reduce the number of feature-maps at transition layers. If a dense block has m feature-maps and we allow the subsequent transition layer to generate m output feature maps, we call our model DenseNet-BC.

A matrix of predictors and a numeric vector with labels are required to be supplied as input data for the training process. This is sufficient information to get started training the model, but we will specify a few more arguments in order to get better control over the training loop during the next step. With batch size, we can control how many observations are passed through at a time, and with epochs = 20, we can instruct the model to pass all of the training data through the training loop 20 times. The study provides an internal validation split at the end of the process by setting validation split of 0.25; this keeps 25% of the data for validation and the results are given in Figure 4.

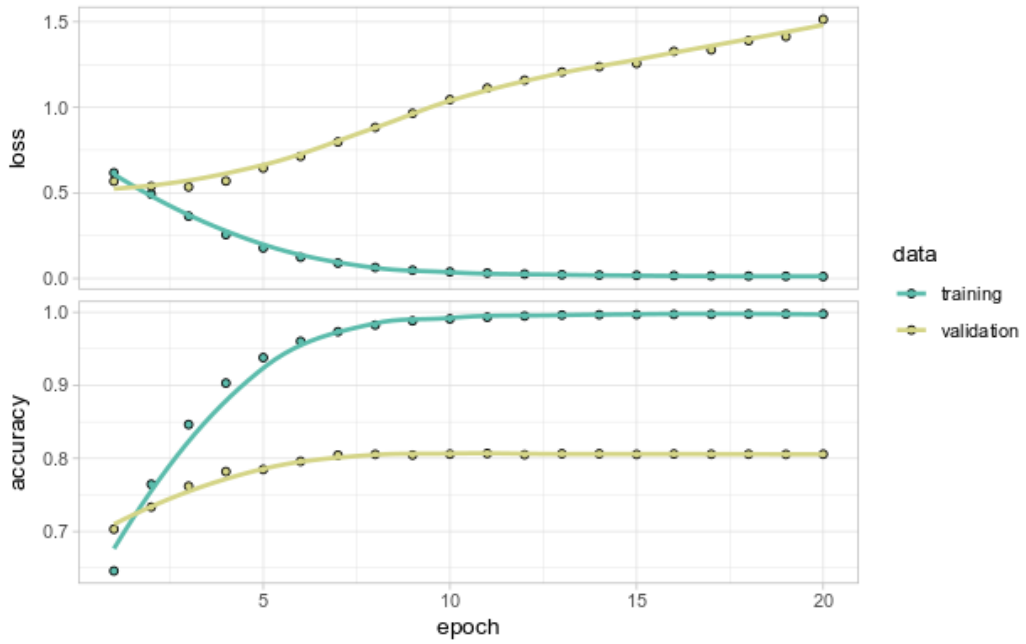

Figure 4: Training and Validation Accuracy of DenseNet

4. Performance Evaluation

Tensor Flow is most likely the most popular deep learning technology. Because HSI data classification is so crucial in RS applications, it was the focus of many of the DL outcomes we examined. HSI processing faces numerous challenges, including high data complexity and often limited training sample numbers. A parametric depth study discovered that adding more layers after a depth of nine caused no improvement in depths ranging from one to fifteen, and that adding more layers after a depth of nine produced no improvement in depths ranging from 1-15.

The settings used for each data set are shown in Table 1.

Table 1: Hyper-parameters

Hyper-parameter	Pavia Centre	Salinas	Indian Pines
Weight decay	0.0002	0.001	0.0005
Number of training steps	40,000	50,000	50,000
Batch normalization decay	0.99	0.99	0.99
Label smoothing	0.1	0	0
Dropout rate	0.2	0.5	0.4
Learning rate	1.28	0.05	0.4
Batch size	2048	128	1024
Number of warm up steps	2000	0	2500
Pseudo label threshold	0.7	0.975	0.95

4.1. Datasets

The researchers examined three different datasets to validate the proposed model with existing CNN architectures, which are given below: Pavia Center, Indian Pines, and Salinas

4.2. Results and Comparisons

The following is a visualisation of the Ground Truth of the Indian Pines dataset:

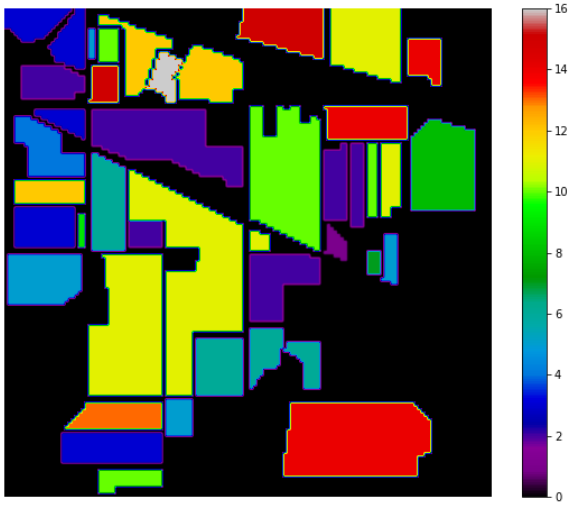

(a) Indian Pines

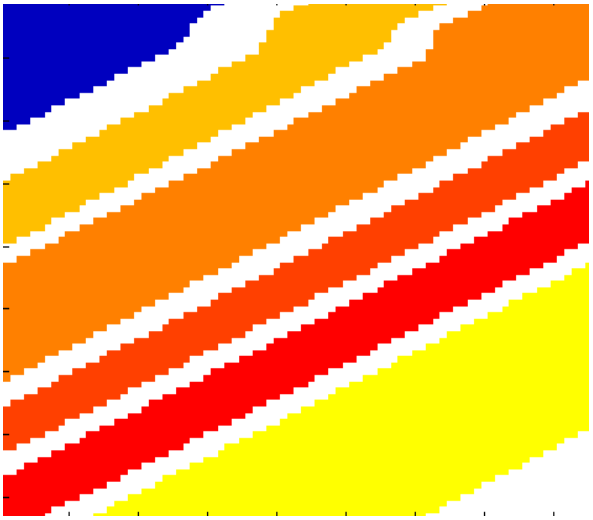

(b) Salinas

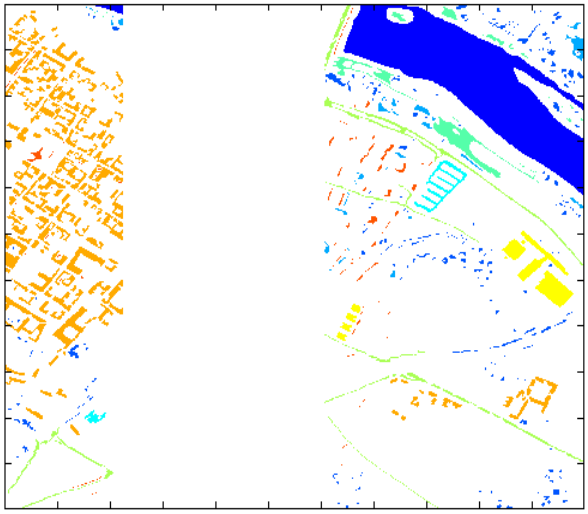

(c) Pavia Center

Figure 5: Ground Truth Visualization

The visualization of the six randomly selected bands over 200 is shown below:

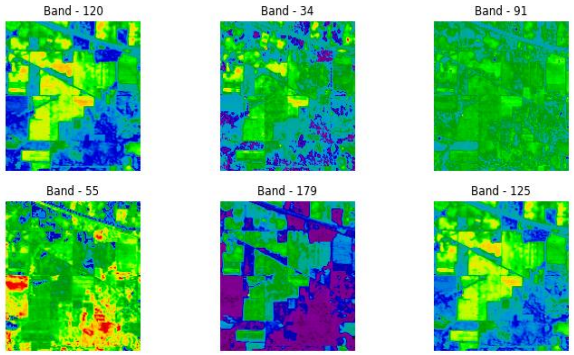

(a) Indian Pines

(b) Salinas

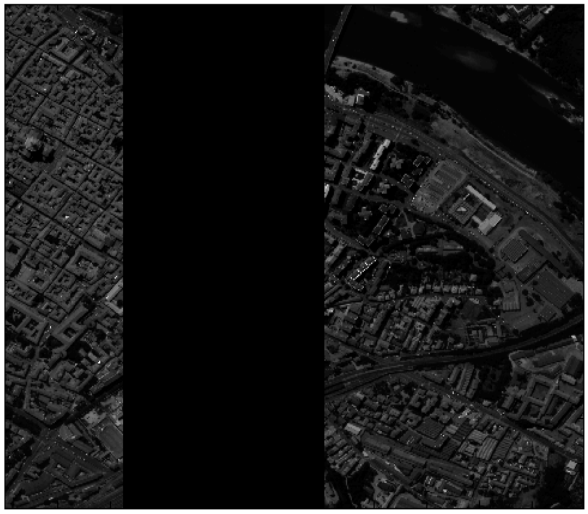

(c) Pavia Center

Figure 6: Indian Pines - Visualization of the Bands

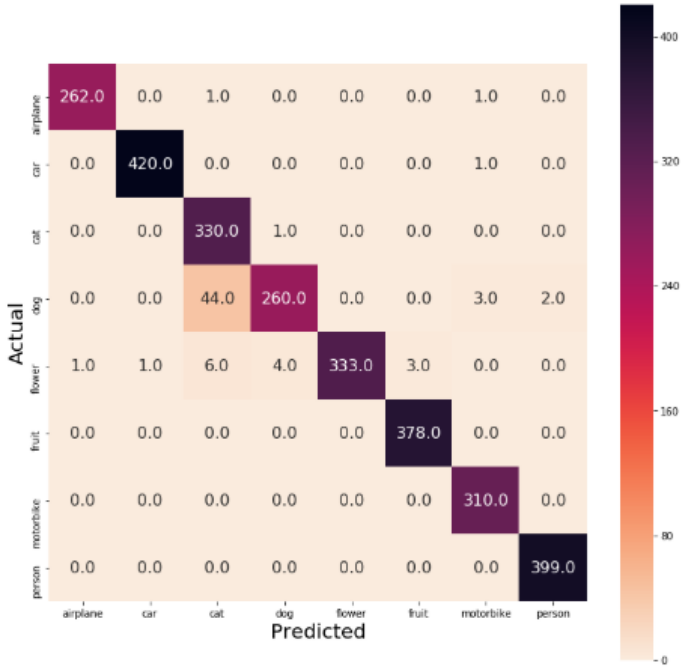

Figure 7: Confusion Matrix (Actual vs. Predicted) for all three datasets

Top-1 and Top-5 accuracy levels on various Dense Net Models during training on the HSI dataset are shown in Table 2. Table 3 shows the HSI Classification Accuracy (mean standard deviation) after ten rounds of training/testing. In the Table 4 discuss about the HSI Classification accuracy during testing with Top-1 and Top-5 accuracy levels with varying parameters of CNN architectures

Table 2: Top-1 and Top-5 accuracy levels on various Dense Net Models on HSI Dataset during training

Method	**Accuracy top-5**	**Accuracy top-1**
ResNet-50	95.45	78.67
ResNet-152	95.96	79.38
Poly Net	96.37	80.20
Inception-v3	96.78	80.92
Xception	97.08	81.64
Inception-v4	96.47	80.71
Inception-resnet-v2	96.67	80.82
ResNeXt-101	98.82	84.40
DenseNet-264	98.72	85.11

Table 3: HSI Classification accuracy (mean± std) over 10 iterations during training/testing

Method	Training (mean ± std)	Testing (mean ± std)
ResNet-50	83.63±0.63	92.81±0.27
ResNet-152	84.13±0.28	94.35±0.47
Poly Net	86.87±0.39	94.65±0.19
Inception-v3	87.94±0.19	93.42±0.36
Xception	92.71±0.02	96.11±0.04
Inception-v4	93.76±0.06	96.73±0.31
Inception-resnet-v2	94.86±0.04	97.17±0.30
ResNeXt-101	94.65±0.04	97.08±0.04
DenseNet-264	**95.74±0.05**	**97.72±0.38**

Table 4: HSI Classification accuracy during testing with Top-1 and Top-5 accuracy levels with varying parameters of CNN architectures

Method	# Params	Training dataset		# Params	Testing dataset	
		Top-1	Top-5		Top-1	Top-5
ResNet-50	26M	77.75	95.14	89M	84.60	98.41
ResNet-152	60M	79.59	95.96	87M	84.70	98.31
Poly Net	34M	79.69	96.06	86M	84.81	98.41
Inception-v3	24M	80.61	96.57	155M	85.42	98.72
Xception	23M	80.82	96.67	557M	86.24	99.23
Inception-v4	48M	81.84	97.19	66M	86.96	99.44
Inception-resnet-v2	56M	81.94	97.29	66M	87.26	99.64
ResNeXt-101	84M	82.76	97.80	480M	87.47	99.74
DenseNet-264	**92M**	83.17	98.00	**300M**	90.59	99.87

5. Conclusion

In this paper, DenseNet-264 is used to classify the HIS characteristics of three independent datasets. The validation of DenseNet-264 reveals that the top-5 DenseNet-264 achieves higher classification accuracy than other current methods with a larger number of parameters. Furthermore, the DenseNet-264 model overcomes the decreased accuracy caused by vanishing gradients in high-level neural networks. As a result, information is kept across longer pathways between the source and destination layers rather than being lost between the levels.

References

[1] Li, S., Song, W., Fang, L., Chen, Y., Ghamisi, P., & Benediktsson, J. A. (2019). Deep learning for hyperspectral image classification: An overview. IEEE Transactions on Geoscience and Remote Sensing, 57(9), 6690-6709.

[2] Zhao, W., & Du, S. (2016). Spectral–spatial feature extraction for hyperspectral image classification: A dimension reduction and deep learning approach. IEEE Transactions on Geoscience and Remote Sensing, 54(8), 4544-4554.

[3] Yang, X., Ye, Y., Li, X., Lau, R. Y., Zhang, X., & Huang, X. (2018). Hyperspectral image classification with deep learning models. IEEE Transactions on Geoscience and Remote Sensing, 56(9), 5408-5423.

[4] Zhong, Z., Li, J., Luo, Z., & Chapman, M. (2017). Spectral–spatial residual network for hyperspectral image classification: A 3-D deep learning framework. IEEE Transactions on Geoscience and Remote Sensing, 56(2), 847-858.

[5] Chen, Y., Wang, Y., Gu, Y., He, X., Ghamisi, P., & Jia, X. (2019). Deep learning ensemble for hyperspectral image classification. IEEE Journal of Selected Topics in Applied Earth Observations and Remote Sensing, 12(6), 1882-1897.

[6] Liu, S., Shi, Q., & Zhang, L. (2020). Few-shot hyperspectral image classification with unknown classes using multitask deep learning. IEEE Transactions on Geoscience and Remote Sensing, 59(6), 5085-5102.

[7] Jia, S., Jiang, S., Lin, Z., Li, N., Xu, M., & Yu, S. (2021). A survey: Deep learning for hyperspectral image classification with few labeled samples. Neurocomputing, 448, 179-204.

[8] Liu, B., Yu, A., Yu, X., Wang, R., Gao, K., & Guo, W. (2020). Deep multiview learning for hyperspectral image classification. IEEE Transactions on Geoscience and Remote Sensing.

[9] Shen, Y., Zhu, S., Chen, C., Du, Q., Xiao, L., Chen, J., & Pan, D. (2020). Efficient deep learning of nonlocal features for hyperspectral image classification. IEEE Transactions on Geoscience and Remote Sensing.

[10] Gong, Z., Zhong, P., & Hu, W. (2020). Statistical loss and analysis for deep learning in hyperspectral image classification. IEEE transactions on neural networks and learning systems, 32(1), 322-333.

[11] Li, H. C., Wang, W. Y., Pan, L., Li, W., Du, Q., & Tao, R. (2020). Robust capsule network based on maximum correntropy criterion for hyperspectral image classification. IEEE Journal of Selected Topics in Applied Earth Observations and Remote Sensing, 13, 738-751.

[12] Yuan, Y., Wang, C., & Jiang, Z. (2021). Proxy-Based Deep Learning Framework for Spectral-Spatial Hyperspectral Image Classification: Efficient and Robust. IEEE Transactions on Geoscience and Remote Sensing.

[13] Yang, B., Li, H., & Guo, Z. (2020). Learning a deep similarity network for hyperspectral image classification. IEEE Journal of Selected Topics in Applied Earth Observations and Remote Sensing, 14, 1482-1496.

[14] Wang, J., Song, X., Sun, L., Huang, W., & Wang, J. (2020). A novel cubic convolutional neural network for hyperspectral image classification. IEEE Journal of Selected Topics in Applied Earth Observations and Remote Sensing, 13, 4133-4148.

[15] Safari, K., Prasad, S., &Labate, D. (2020). A multiscale deep learning approach for high-resolution hyperspectral image classification. IEEE Geoscience and Remote Sensing Letters, 18(1), 167-171.

[16] Liu, B., Gao, K., Yu, A., Guo, W., Wang, R., &Zuo, X. (2020). Semisupervised graph convolutional network for hyperspectral image classification. Journal of Applied Remote Sensing, 14(2), 026516.

[17] Lei, Z., Zeng, Y., Liu, P., &Su, X. (2021). Active deep learning for hyperspectral image classification with uncertainty learning. IEEE Geoscience and Remote Sensing Letters.